AGU PUBLICATIONS

Geophysical Research Letters

RESEARCH LETTER
10.1002/2016GL069412

Key Points:
- Crater size–frequency distributions for all major volcanic plains units on Mercury are similar
- None of these units has a model age younger than about 3.5 Ga
- Interior cooling and contraction likely inhibited widespread plains volcanism on Mercury thereafter

Correspondence to:
P. K. Byrne,
paul.byrne@ncsu.edu

Citation:
Byrne, P. K., L. R. Ostrach, C. I. Fassett, C. R. Chapman, B. W. Denevi, A. J. Evans, C. Klimczak, M. E. Banks, J. W. Head, and S. C. Solomon (2016), Widespread effusive volcanism on Mercury likely ended by about 3.5 Ga, *Geophys. Res. Lett.*, *43*, 7408–7416, doi:10.1002/2016GL069412.

Received 2 MAY 2016
Accepted 24 JUN 2016
Accepted article online 27 JUN 2016
Published online 21 JUL 2016

Widespread effusive volcanism on Mercury likely ended by about 3.5 Ga

Paul K. Byrne[1,2], Lillian R. Ostrach[3], Caleb I. Fassett[4], Clark R. Chapman[5], Brett W. Denevi[6], Alexander J. Evans[5,7], Christian Klimczak[2,8], Maria E. Banks[9,10], James W. Head[11], and Sean C. Solomon[2,7]

[1]Planetary Research Group, Department of Marine, Earth, and Atmospheric Sciences, North Carolina State University at Raleigh, Raleigh, North Carolina, USA, [2]Department of Terrestrial Magnetism, Carnegie Institution of Washington, Washington, District of Columbia, USA, [3]Solar System Exploration Division, NASA Goddard Space Flight Center, Greenbelt, Maryland, USA, [4]Department of Astronomy, Mount Holyoke College, South Hadley, Massachusetts, USA, [5]Department of Space Studies, Southwest Research Institute, Boulder, Colorado, USA, [6]The Johns Hopkins University Applied Physics Laboratory, Laurel, Maryland, USA, [7]Lamont-Doherty Earth Observatory, Columbia University, Palisades, New York, USA, [8]Department of Geology, University of Georgia, Athens, Georgia, USA, [9]Center for Earth and Planetary Studies, Smithsonian National Air and Space Museum, Washington, District of Columbia, USA, [10]Planetary Science Institute, Tucson, Arizona, USA, [11]Department of Earth, Environmental and Planetary Sciences, Brown University, Providence, Rhode Island, USA

Abstract Crater size–frequency analyses have shown that the largest volcanic plains deposits on Mercury were emplaced around 3.7 Ga, as determined with recent model production function chronologies for impact crater formation on that planet. To test the hypothesis that all major smooth plains on Mercury were emplaced by about that time, we determined crater size–frequency distributions for the nine next-largest deposits, which we interpret also as volcanic. Our crater density measurements are consistent with those of the largest areas of smooth plains on the planet. Model ages based on recent crater production rate estimates for Mercury imply that the main phase of plains volcanism on Mercury had ended by ~3.5 Ga, with only small-scale volcanism enduring beyond that time. Cessation of widespread effusive volcanism is attributable to interior cooling and contraction of the innermost planet.

1. Introduction

The importance of volcanism in the geological development of Mercury was suggested by data from the Mariner 10 mission in the 1970s [e.g., *Strom et al.*, 1975] and was affirmed by observations of the planet acquired by the MErcury Surface, Space ENvironment, GEochemistry, and Ranging (MESSENGER) spacecraft during three flybys in 2008–2010 [*Head et al.*, 2008, 2009a, 2009b]. Diffuse-edged deposits with a distinct reddish color, often found in association with irregularly shaped depressions lacking raised rims, provided evidence for past episodes of explosive volcanism [*Head et al.*, 2008; *Murchie et al.*, 2008; *Robinson et al.*, 2008; *Head et al.*, 2009a; *Kerber et al.*, 2009]. The smooth plains units identified originally in the hemisphere imaged by Mariner 10 were found to occur across the planet [*Denevi et al.*, 2009], with embayment relations, ponding in lowlands, the presence of partially or nearly entirely infilled craters (i.e., "ghost craters") within these units, and in many instances spectral contrast with surrounding terrain indicating that the vast majority of these smooth plains by area are volcanic deposits emplaced effusively [e.g., *Head et al.*, 2009a].

Image data from the orbital phase of MESSENGER operations allowed the global distribution of smooth plains units to be characterized [*Denevi et al.*, 2013]. Occupying ~27% of the planet's surface, these plains are sparsely cratered relative to other terrain, are essentially level at horizontal baselines less than ~100 km, and generally have clearly defined boundaries [*Trask and Guest*, 1975]. The largest single deposit is located at middle to high northern latitudes and so is termed the northern smooth plains (NSP); with an area of 5.6×10^6 km^2 (see Table S1), these plains cover about 7% of Mercury's surface [*Ostrach et al.*, 2015]. Other large deposits in the northern hemisphere include the Caloris interior and exterior plains, with portions of the latter possibly including basin ejecta material [*Denevi et al.*, 2009, 2013; *Fassett et al.*, 2009]. In the southern hemisphere, the plains interior to the Rembrandt basin form the largest volcanic deposit. Crater size–frequency analyses have shown that the NSP and the Caloris and Rembrandt interior plains were emplaced at around 3.7 Ga [*Fassett et al.*, 2009; *Head et al.*, 2011; *Strom et al.*, 2011; *Denevi et al.*, 2013; *Ferrari et al.*, 2014; *Ostrach et al.*, 2015] for many of the published chronology models for Mercury [e.g., *Marchi et al.*, 2009], including the

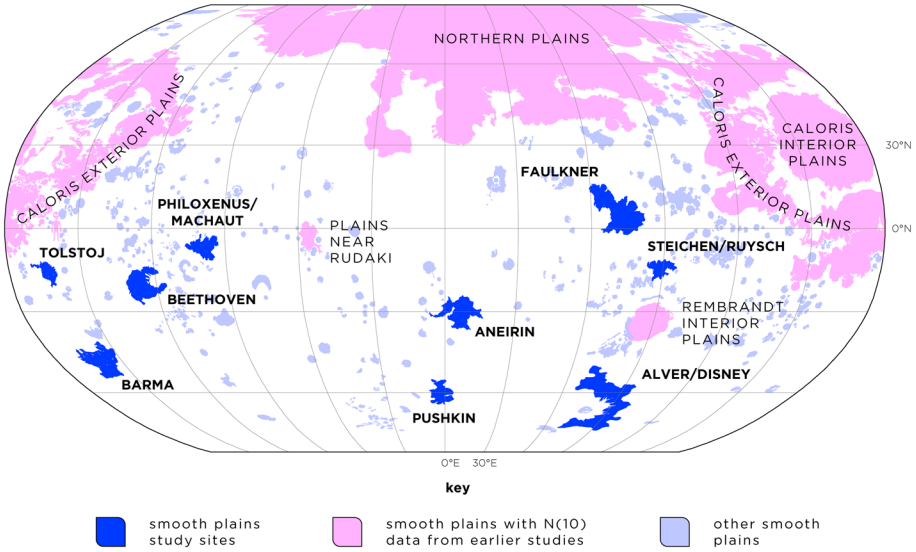

Figure 1. Mapped smooth plains deposits on Mercury [after *Denevi et al.*, 2013]. The nine sites we consider in this study are shown in blue. Other plains units for which areal crater density measurements have been reported earlier [*Fassett et al.*, 2009; *Denevi et al.*, 2013; *Ostrach et al.*, 2015; *Whitten et al.*, 2014] are shown in pink. Remaining smooth plains deposits are in lavender. The map is in a Robinson projection centered at 0°E; the graticule is in 30° increments of latitude and longitude.

model of *Le Feuvre and Wieczorek* [2011] that incorporates the effects of a porous megaregolith. Further, the areal density of impact craters for an additional large smooth plains deposit on Mercury—southeast of the Rachmaninoff basin, near Faulkner crater—is comparable to those for the NSP and the Caloris interior plains [*Fassett et al.*, 2009; *Denevi et al.*, 2013; *Whitten et al.*, 2014; *Ostrach et al.*, 2015], implying that this additional unit is similar in age.

It may be, then, that all major volcanic smooth plains units on Mercury were emplaced by about this time, early in the planet's history—in contrast to the protracted (i.e., multibillion-year) records of effusive volcanism on Earth [e.g., *Bryan et al.*, 2010], Mars [e.g., *Carr and Head*, 2010], and Venus [e.g., *Ivanov and Head*, 2013]. To test this hypothesis, we determined crater size–frequency distributions (SFDs) for nine large smooth plains units on Mercury; all but one of which are in the planet's southern hemisphere (Figure 1). (These sites are described in the supporting information.) We interpret all of these deposits as likely to be volcanic in nature on the same basis by which volcanic units were identified on Mercury in earlier studies [e.g., *Head et al.*, 2009a, 2011]: each appears to have infilled preexisting lowlands, portions of each are spectrally distinct from neighboring terrain, and all host ghost craters. This latter crater population indicates that, at each location, considerable geological time elapsed between formation of the underlying basement and these plains.

2. Methods

The Mercury Dual Imaging System [*Hawkins et al.*, 2007] composite narrow- and wide-angle camera global image mosaic at 250 m/pixel resolution [cf. *Chabot et al.*, 2016] served as the base map for our crater analysis. Each of the nine sites was delineated with the mapping classification scheme employed by *Denevi et al.* [2013]. Whereas that global survey of smooth plains was conducted at a scale of 1:1.25 M, we mapped each site in this work at a scale of 1:800,000, so minor variations exist between deposit outlines here and those in the earlier work. All image data were analyzed within an ESRI® ArcMap™ 10.1 geographical information system.

To determine the SFD of primary impact craters at each site, we used the CraterTools extension [*Kneissl et al.*, 2011] for ArcMap 10. We included only craters $\geq$4 km in diameter, given the prospect of contamination by secondaries at diameters as great as 10 km [*Strom et al.*, 2008]. We excluded obvious secondary craters (and their associated areas) on the basis of their occurrence in clusters or chains, but far-field secondaries cannot be readily recognized, and the contamination of counts by unrecognized secondaries is expected to become increasingly severe at smaller diameters.

We report crater density measurements for each site in terms of $N(4)$ and $N(10)$ values, where $N(D)$ is the number of craters greater than diameter D (in km) per 10^6 km^2 area [e.g., *Ostrach et al.*, 2015]. This approach has the benefit of allowing comparisons between our spatial density results and those of previous studies [e.g., *Denevi et al.*, 2013]. (For this reason we also give $N(20)$ values for those sites where craters ≥20 km in diameter are present.) Stated errors are the standard deviation for each value of $N(D)$, taken to be the square root of the number of craters per diameter bin per 10^6 km^2 [*Crater Analysis Techniques Working Group*, 1979].

Absolute model ages were determined for each site with the 2016-06-13 compiled version of the Craterstats program [e.g., *Michael and Neukum*, 2010], using the model production function (MPF) and chronology of *Le Feuvre and Wieczorek* [2011]. We selected this MPF over older chronologies [e.g., *Strom and Neukum*, 1988; *Neukum et al.*, 2001] because it incorporates revised estimates both for crater scaling and for the impact flux at Mercury, as well as two impactor populations and target-specific properties [*Le Feuvre and Wieczorek*, 2011]. We obtained model ages for our measured crater size–frequency distributions by Poisson timing analysis [*Michael et al.*, 2016], given scaling relations between impactor diameter and crater diameter for both porous and nonporous targets [*Holsapple and Housen*, 2007] (where porous-target scaling is intended to correspond to a heavily fractured megaregolith [*Le Feuvre and Wieczorek*, 2011]).

We used the full range of crater diameters (i.e., ≥4 km) to determine absolute model ages for each site. However, because secondary craters become increasingly more abundant at diameters below 10 km on Mercury and have been suggested to become prevalent in crater populations at diameters below 7 km [*Strom et al.*, 2008], we also calculated model ages for craters ≥10 km in diameter at each site. The determination of model ages with Poisson timing analysis returns plots of model age uncertainty as a probability density function, marked by vertical lines at the 50 and 50 ± 34 percentiles [*Michael et al.*, 2016]. (These are shown in the top right of each plot in Figures 2, S1, and S2.) Note that because systematic uncertainties in the chronology model are much larger than errors from counting statistics (by at least several hundred million years) and are not very well constrained, we quote model ages only to two significant figures.

3. Results

3.1. Crater Size–Frequency Distributions

Spatial density values for craters ≥4 km, ≥10 km, and ≥20 km in diameter (i.e., $N(4)$, $N(10)$, and $N(20)$, respectively) superposing the smooth plains at each site are given in Table 1. We focus here on our $N(10)$ measurements, as this quantity is the most widely quoted areal density value with which we can compare our results. We find a span of $N(10)$ values of 29 ± 21 to 145 ± 23, which encompasses the range of corresponding values for previously assessed smooth plains deposits on Mercury (Table S1). Of note, the greatest areal density measurement for craters ≥10 km in diameter found here, for the plains between the Alver and Disney craters (145 ± 23), is close to the lowest $N(10)$ values reported for a representative intercrater plains unit to the east of Tolstoj (154 ± 34) [*Whitten et al.*, 2014]. Additionally, the $N(10)$ values that we find for Beethoven and Faulkner are similar (in that errors overlap) to published values for these plains units. For example, *Denevi et al.* [2013] and *Whitten et al.* [2014] calculated $N(10)$ values of 82 ± 19 and 77 ± 24, respectively, for the plains within the Beethoven basin; we find $N(10) = 92 \pm 22$ for that unit. And for the plains unit we termed Faulkner, where $N(10) = 34 \pm 10$, *Denevi et al.* [2013] found $N(10) = 58 \pm 18$ (and labeled those plains "South of Rachmaninoff"). Together, the $N(10)$ values we report point to a continued period of volcanic emplacement, from those that constitute Mercury's intercrater plains to the least cratered smooth plains units preserved on the planet, with no clear spatial partitioning of activity (e.g., we find similar values for plains units in both the eastern and western hemispheres).

3.2. Absolute Model Ages

The MPF of *Le Feuvre and Wieczorek* [2011] with porous-target scaling for our crater SFD data for craters ≥4 km in diameter at each site returns model ages by Poisson timing analysis of about 3.5–3.8 Gyr; when determined for each site for craters ≥10 km in diameter, that same isochron gives a similar model age range (albeit with an age of 2.6 Ga for one location for which crater statistics are poor; Table 1). In contrast, use of the *Le Feuvre and Wieczorek* [2011] MPF with non-porous-target scaling to our measurements (i.e., using "hard-rock" target properties to derive crater diameter from impactor diameter [*Holsapple and Housen*, 2007]) yields by

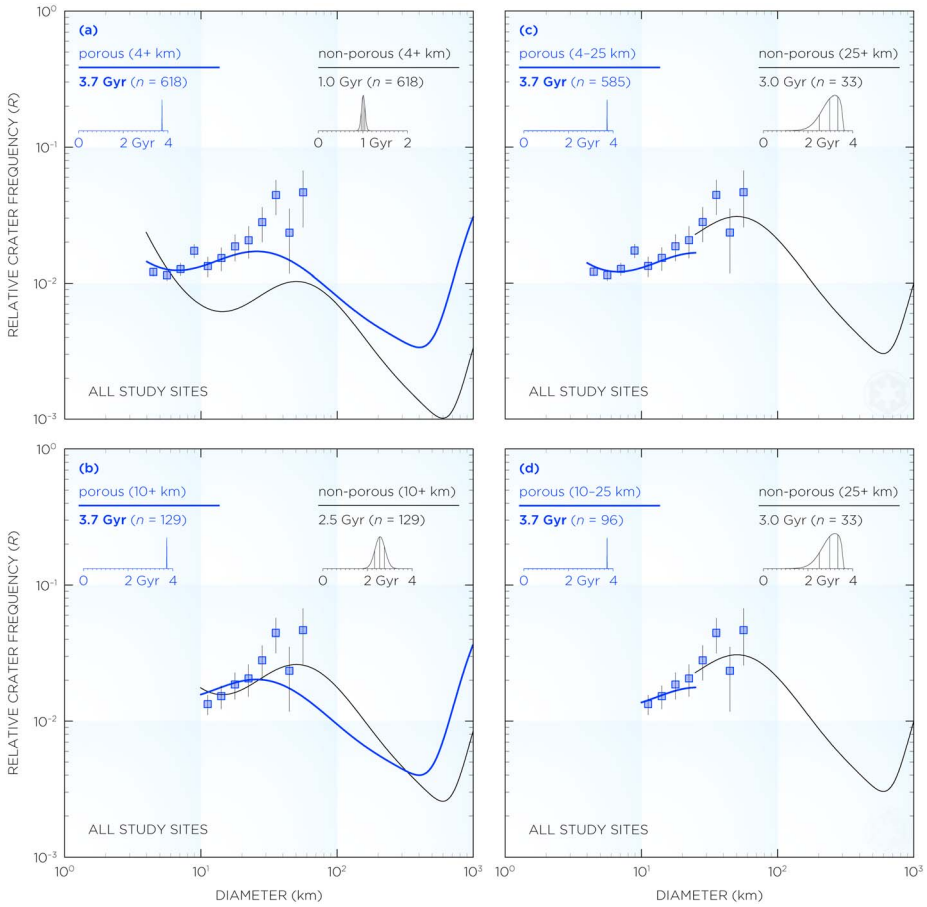

Figure 2. Aggregate *R* plots for the craters in our study. The isochrons for porous-target and non-porous-target scaling of *Le Feuvre and Wieczorek* [2011] are shown with solid blue and solid black lines, respectively. Model ages derived by Poisson timing analysis [*Michael et al.*, 2016] are also shown; so, too, are plots of the associated uncertainty as probability density functions. (a) *R* plot for the 618 craters ≥4 km in diameter. (b) *R* plot for the 129 craters ≥10 km in diameter. (c) *R* plot for the 618 craters ≥4 km in diameter, with the isochron for porous-target scaling for craters 4–25 km in diameter ($n = 585$) and the isochron for non-porous-target scaling for craters 25 km in diameter and above ($n = 33$). (d) *R* plot for the 129 craters ≥10 km in diameter, with the isochron for porous-target scaling for craters 10–25 km in diameter ($n = 96$) and the isochron for non-porous-target scaling for craters 25 km in diameter and above, as in Figure 2c.

Table 1. Location, Count Area, Crater Spatial Density, and Model Age for Each of the Sites in This Study

							Model Age (Gyr)[b]	
Site	Latitude (°N)	Longitude (°E)	Area (km^2)	$N(4)$[a]	$N(10)$[a]	$N(20)$[a]	$N(4)$	$N(10)$
Alver/Disney	−64.09	84.17	2.63×10^5	517 ± 44	145 ± 23	65 ± 16	3.7	3.8
Aneirin	−30.22	6.48	1.80×10^5	311 ± 42	72 ± 20	22 ± 11	3.7	3.7
Barma	−47.99	−159.03	1.59×10^5	446 ± 53	138 ± 29	44 ± 17	3.7	3.8
Beethoven	−20.37	−125.43	1.95×10^5	595 ± 55	92 ± 22	31 ± 13	3.8	3.7
Faulkner	3.27	71.04	3.48×10^5	391 ± 34	34 ± 10	14 ± 6	3.7	3.2
Philoxenus/Machaut	−6.73	−98.55	1.15×10^5	365 ± 56	130 ± 34	35 ± 17	3.7	3.8
Pushkin	−60.26	−1.70	6.43×10^4	327 ± 71	47 ± 27	n/a[c]	3.7	3.0
Steichen/Ruysch	−14.38	89.25	7.95×10^4	314 ± 63	75 ± 31	25 ± 18	3.7	3.6
Tolstoj	−15.81	−164.07	6.84×10^4	234 ± 58	29 ± 21	15 ± 15	3.5	2.6

[a]We give confidence intervals for our N(*D*) values of ±1 standard deviation, taken to equal the square root of the number of craters counted, normalized to an area of 10^6 km^2 [e.g., *Crater Analysis Techniques Working Group*, 1979; *Fassett et al.*, 2009].
[b]These ages are derived by Poisson timing analysis [*Michael et al.*, 2016] for the porous-target scaling of *Le Feuvre and Wieczorek* [2011] applied to our crater data.
[c]This site has no post-plains craters 20 km or greater in diameter.

Poisson timing analysis a model curve considerably different from the trend of our data for crater diameters both ≥4 km and ≥10 km as well as the MPF isochron with porous-target scaling.

This difference is illustrated in Figure 2, where plots of relative crater frequency versus crater diameter (i.e., *R* plots [cf. *Crater Analysis Techniques Working Group*, 1979]) are shown. Here the non-porous-target isochron returns a model age by Poisson timing analysis of 1.0 Gyr for ≥4 km diameter craters at all nine sites together ($n = 618$); in contrast, the porous-target isochron gives a model age of 3.7 Gyr for this aggregate crater population (Figure 2a). When applied to the SFD data for all ≥10 km diameter craters ($n = 129$), the non-porous-target isochron gives a model age by Poisson calculation of 2.5 Gyr, whereas the porous-target isochron again returns a model age of 3.7 Gyr (Figure 2b).

We note, however, that the isochron for non-porous-target scaling matches well qualitatively the aggregate population of craters with diameters ≥25 km ($n = 33$), with a model age by Poisson timing analysis of 3.0 Gyr (Figures 2c and 2d), whereas the porous-target isochron is more consistent with craters below this diameter, returning a model age of 3.7 Gyr for both 4–25 km diameter craters ($n = 585$; Figure 2c) and 10–25 km diameter craters ($n = 96$; Figure 2d). Nonetheless, we consider age estimates for each site calculated by Poisson calculation with the porous-target scaling model more robust because they better match the shape of the observed crater SFD, where we have the best counting statistics (i.e., at crater diameters <25 km) than estimates with the non-porous-target scaling model. We show *R* plots of relative crater frequency versus crater diameter, with model ages derived by Poisson timing analysis, for the porous- and non-porous-target scaling isochrons of *Le Feuvre and Wieczorek* [2011], for craters ≥4 km in diameter at each site in Figure S1 and for craters ≥10 km in diameter at each site in Figure S2.

4. Discussion

Morphological evidence indicates that much of Mercury's crust was emplaced as effusive volcanic deposits. Progressive cratering (especially secondary cratering) then transformed what were originally smooth plains into terrain with textures that correspond to that of older intercrater plains [e.g., *Spudis and Guest*, 1988; *Denevi et al*., 2013; *Whitten et al*., 2014]. Global surveys of Mercury's impact crater population indicate a spatially variable but generally lower areal density of craters ~20–50 km in diameter in the more heavily cratered regions of the planet than in the lunar highlands, consistent with removal of craters of that size range at least in part by volcanic resurfacing [*Strom and Neukum*, 1988; *Fassett et al*., 2011; *Strom et al*., 2011; *Fassett et al*., 2012]. And crater statistics for the most heavily cratered terrain on Mercury suggest that the oldest preserved portions of the surface date to about 4.0–4.1 Ga, supporting further the inference that volcanic resurfacing was a dominant process early in the planet's history, likely in concert with heavy impact bombardment [*Marchi et al*., 2013].

The *N*(10) values we report here for these nine sites are similar to those for the largest expanses of effusive volcanic deposits on Mercury—the NSP, Caloris Planitia and the smooth plains exterior to Caloris, and the Rembrandt interior plains [*Fassett et al*., 2009; *Head et al*., 2011; *Strom et al*., 2011; *Denevi et al*., 2013; *Ferrari et al*., 2014; *Ostrach et al*., 2015]—as well as for smaller units, including smooth plains near Rudaki crater [*Denevi et al*., 2013] (Tables 1 and S1). Further, our results for the Beethoven and Faulkner sites resemble *N*(10) values for those deposits reported earlier [e.g., *Denevi et al*., 2013; *Whitten et al*., 2014]. That the highest *N*(10) value we report is similar to that of an intercrater plains unit documented by *Whitten et al.* [2014] supports the scenario, proposed by those and other authors, under which progressive cratering of smooth plains units eventually renders them sufficiently textured so as to be classified as intercrater plains.

With the recent crater chronology for Mercury of *Le Feuvre and Wieczorek* [2011] for porous-target scaling, our crater spatial density data both for craters ≥4 km and ≥10 km in diameter yield absolute model ages by Poisson timing analysis that span a relatively narrow temporal window. The broad similarity in model ages for both crater diameter ranges may imply that the SFDs of these sites are not strongly contaminated by unrecognized secondary craters larger than 4 km in diameter. Additionally, although we prefer the model age estimates calculated with porous-target scaling to those found with non-porous-target scaling, the observed size-dependent difference between the model isochrons and the data is considerable (Figure 2). This difference may be plausibly explained by a sharp increase with depth in the effective strength of Mercury's lithosphere (as suggested by, e.g., *Massironi et al.* [2009]). These data could therefore suggest that the *Le Feuvre and Wieczorek* [2011] isochrons for Mercury together reflect a change in the mechanical

properties of the lithosphere at some depth, perhaps ~10 km for final crater diameters >25 km in smooth plains across Mercury.

Importantly, there are numerous uncertainties inherent to the crater-derived absolute model ages. The possibility of unrecognized differences in retention rates of craters of different diameters, secular variations in impactor populations, or errors in scaling laws for impact cratering and ejecta require that calculated absolute model ages be assessed with care and not be overinterpreted. Nonetheless, for the method of deriving model ages we adopt here (i.e., the porous-target-scaling isochron of *Le Feuvre and Wieczorek* [2011] for craters ≥4 km by Poisson timing analysis), no deposit we examined has a model age resolvably younger than about 3.5 Gyr. All such units are also consistent with the crater density and ages of the NSP, the Caloris interior and exterior plains, and the Rembrandt interior plains of ~3.6–3.8 Gyr [e.g., *Fassett et al*., 2009; *Head et al*., 2011; *Denevi et al*., 2013; *Ostrach et al*., 2015]. Further, an independent model production function for Mercury [*Marchi et al*., 2013] gives similar results—our areal density data plotted on their Figure 3 returns ages of ~3.6–3.9 Gyr. Taken together, then, morphological observations, crater size–frequency distribution data, and model age results suggest that widespread effusive volcanism on Mercury, a key process by which the crust developed, came to an end globally over a geologically short interval within about the first 20% of the age of the planet.

The cessation of widespread plains volcanism may reflect a waning magma supply as a consequence of secular interior cooling, as suggested by thermochemical evolution models for Mercury [*Michel et al*., 2013; *Tosi et al*., 2013; *Evans et al*., 2015]. Although chemically homogeneous models of Mercury's interior indicate that extensive magmagenesis could have lasted until around 2 Ga [*Tosi et al*., 2013], post-magma-ocean models suggest that a mantle with compositional stratification would have likely suppressed this extensive melting phase by about 3.5 Ga [*Evans et al*., 2015], contemporaneous with what observations suggest is the end of widespread plains emplacement.

Secular cooling may also have played a key role in the cessation of plains volcanism on Mercury in a different manner. The surface of Mercury hosts thousands of tectonic landforms, including lobate scarps and wrinkle ridges, which are interpreted to have formed in response to horizontal shortening that resulted from a reduction in planetary volume as the interior cooled and contracted [e.g., *Strom et al*., 1975]. Together these landforms have accommodated a decrease in planetary radius by as much as 7 km [*Byrne et al*., 2014]. In a tectonic regime governed by global contraction, the least compressive stresses act vertically and are governed by the overburden, whereas the most compressive stresses act in the horizontal plane. Such a stress field is compatible with the formation of thrust faults, once the brittle strength of the lithosphere is reached [e.g., *Klimczak*, 2015]. Yet a globally compressive stress state where the magnitude of the horizontal stress component exceeds that of the vertical component inhibits the vertical ascent of magma [e.g., *Glazner*, 1991; *Hamilton*, 1995; *Watanabe et al*., 1999] and so is not readily conducive to widespread effusive volcanism [e.g., *Solomon*, 1978; *Marrett and Emmerman*, 1992]. Under such a stress state, magmas are much more likely to propagate laterally, forming sills. Widespread effusive volcanism on Mercury is therefore not expected to occur after the onset of global contraction [*Wilson and Head*, 2008].

Superposition relations between impact craters and lobate scarps indicate that global contraction was underway by the time that at least some effusive volcanic activity was taking place. The oldest craters observed to superpose scarp segments on Mercury are estimated to have formed after the end of the late heavy bombardment, during the Calorian system; this assessment of age is made on the basis that these craters are themselves superposed by multiple other craters and are moderately degraded with subdued ejecta blankets and moderately subdued and rounded rim crests [*Spudis and Guest*, 1988; *Banks et al*., 2015]. Observations of Calorian craters superposing scarps require, by definition, that brittle failure of Mercury's surface at least regionally was underway at some point after the formation of the Caloris basin, subsequently a site of extensive effusive volcanism.

It has long been noted that many volcanic smooth plains units on Mercury, including the Caloris interior plains and those in Beethoven, Rembrandt, and Tolstoj, are situated within preexisting impact basins and craters [e.g., *Strom et al*., 1975; *Fassett et al*., 2012]. So, too, are many smaller areas of smooth plains across the planet [*Denevi et al*., 2013], at least some of which are likely volcanic [*Prockter et al*., 2010; *Marchi et al*., 2011]. This collocation of many of the youngest effusive volcanic units on Mercury with impact structures is consistent with predictions for a planet undergoing contraction from secular interior cooling [*Solomon*, 1978]. Although the importance to volcanism of impacts on Earth has been controversial

[*Ivanov and Melosh*, 2003; *Glickson*, 2004; *Elkins-Tanton and Hager*, 2005], the impact process removes overburden, promotes subsurface uplift, relaxes preexisting stresses, substantially fractures the lithosphere and thus provides pathways along which magma may ascend [e.g., *Klimczak*, 2015], and introduces heat into the mantle that may trigger the production of melt [*Roberts and Barnouin*, 2012]. Impact structures are therefore prime sites for late-stage eruptions in a tectonic regime otherwise generally unfavorable to extrusive activity. The sharp reduction in the rate of bombardment at around 3.9–3.8 Ga may therefore have played at least some part in the tapering of effusive volcanism thereafter.

Importantly, the cessation of large-scale effusive volcanism on Mercury did not spell the end of volcanic activity on the planet as a whole. At least two other smooth plains units have been identified as potentially younger than ~1 Gyr, far younger than both the smallest and the youngest deposits we examined here (the plains near Pushkin and those within Tolstoj, respectively; see Table 1). However, both of these substantially younger deposits are situated within the peak rings of medium-sized impact basins: the Rachmaninoff basin (290 km diameter) [*Prockter et al*., 2010] and the Raditladi basin (265 km diameter) [*Marchi et al*., 2011], such that each of these deposits is $\sim 1.4 \times 10^4$ km^2 in area. Further, it is possible that the deposit within Raditladi basin, which may be only hundreds of millions years old, is impact melt [*Marchi et al*., 2011]. Nonetheless, the size and location of each of these young deposits is consistent with the effects of global contraction, whereby plains volcanism is limited in volume and is collocated with areas of preexisting weakness (i.e., impact features). Other deposits on Mercury may have similar, relatively young ages, but our survey indicates that no such deposit is greater than $\sim 6 \times 10^4$ km^2 in area.

The onset of global contraction did not similarly inhibit explosive volcanic activity on Mercury, however. Irregular depressions morphologically dissimilar to impact craters and often surrounded by diffuse deposits have been interpreted as pyroclastic vents [*Head et al*., 2008; *Kerber et al*., 2009, 2011; *Goudge et al*., 2014; *Thomas et al*., 2014]. Several of these vents superpose and thus postdate Caloris Planitia [*Head et al*., 2008], and at least one example (that which cuts the wall terraces within the 26 km diameter Kuniyoshi crater) may also potentially be as young as ~1 Gyr [*Thomas et al*., 2014]. Volatiles provide the primary driving force for explosive volcanic eruptions [*Cashman*, 2004], and volatile-rich melts are more capable of ascent and eruption than effusive magmas. Nonetheless, the majority of pyroclastic deposits on Mercury are collocated with sites of preexisting weakness in the lithosphere, including the heavily fractured central peaks, peak rings, and rims of impact craters and basins [e.g., *Kerber et al*., 2011], as well as along the surface traces of thrust faults thought to underlie lobate scarps [e.g., *Goudge et al*., 2014]. Fractures and faults, especially if critically stressed, may act as conduits for the upward migration of volatile-rich magmas [*Klimczak et al*., 2013], and so these spatial relations indicate that the history of explosive volcanism on Mercury has also been influenced, at least in part, by global contraction.

5. Concluding Remarks

Crater spatial density and model age analyses have shown that emplacement at nine major sites of effusive volcanism on Mercury ceased by about 3.5 Ga. The data we report for these nine sites match corresponding crater spatial density and model age values for the largest volcanic smooth plains on the planet. Our results therefore indicate that all major plains volcanism on Mercury, i.e., for sites $\geq 1 \times 10^5$ km^2 in area, ended within approximately the first billion years after planet formation. This history of plains volcanism is strikingly different from that of Earth, Mars, and Venus, on which continuing (if episodic) effusive volcanic activity has occurred within the last billion years. Notably, in contrast, the history of plains volcanism on the Moon may mirror that of Mercury: although some lunar basalts are thought to have erupted as recently as 1.2 Ga, they are of very limited areal extent (e.g., 10^3–10^4 km^2) [*Hiesinger et al*., 2003] and are entirely confined to preexisting impact basins.

The cessation of widespread plains volcanism on Mercury is likely a function of secular interior cooling, which would serve to reduce the rate of magmagenesis and result in global planetary contraction, in turn placing the lithosphere into a stress state adverse to the ascent and eruption of magma. Notably, thermochemical evolution models and superposition observations of impact craters and shortening landforms indicate that both a reduction in magma production rates and the onset of global contraction were underway by around 3.7–3.5 Ga—the approximate time frame over which large-scale effusive volcanism on Mercury came to an end globally. That only much smaller volumes of smooth plains units and pyroclastic deposits have resolvably

younger model or stratigraphic ages, and that these deposits are situated within or proximal to impact craters and other sites of preexisting crustal weakness, supports a scenario under which secular cooling effectively ended the bulk of volcanic activity on the innermost planet. With the increasing number of terrestrial planets identified in extrasolar planetary systems [e.g., *Barclay et al*., 2013], Mercury may come to serve as a case study with which to understand the global cooling and volcanic histories of rocky, one-plate planets in general.

Acknowledgments
We thank David A. Rothery and an anonymous reviewer for their comments that helped improve the paper. We also thank Greg Michael for his help with the application of Poisson timing analysis with Craterstats to this study. The MESSENGER project is supported by the NASA Discovery Program under contracts NASW-00002 to the Carnegie Institution of Washington and NAS5-97271 to The Johns Hopkins University Applied Physics Laboratory. P.K.B. acknowledges support from North Carolina State University faculty start-up funds. C.I.F. is supported on this study by NASA grant NNX14AR88G. All MESSENGER data used in this paper are publicly available at the NASA Planetary Data System (PDS). This research made use of NASA's PDS and Astrophysics Data System.

References

Banks, M. E., Z. Xiao, T. R. Watters, R. G. Strom, S. E. Braden, C. R. Chapman, S. C. Solomon, C. Klimczak, and P. K. Byrne (2015), Duration of activity on lobate-scarp thrust faults on Mercury, *J. Geophys. Res. Planets*, *120*, 1751–1762, doi:10.1002/2015JE004828.

Barclay, T., et al. (2013), A sub-Mercury-sized exoplanet, *Nature*, *494*, 452–454, doi:10.1038/nature11914.

Bryan, S. E., I. U. Peate, D. W. Peate, S. Self, D. A. Jerram, M. R. Mawby, J. S. Marsh, and J. A. Miller (2010), The largest volcanic eruptions on Earth, *Earth Sci. Rev.*, *102*, 207–229, doi:10.1016/j.earscirev.2010.07.001.

Byrne, P. K., C. Klimczak, A. M. C. Şengör, S. C. Solomon, T. R. Watters, and S. A. Hauck II (2014), Mercury's global contraction much greater than earlier estimates, *Nat. Geosci.*, *7*, 301–307, doi:10.1038/ngeo2097.

Carr, M. H., and J. W. Head (2010), Geologic history of Mars, *Earth Planet. Sci. Lett.*, *294*, 185–203, doi:10.1016/j.epsl.2009.06.042.

Cashman, K. V. (2004), Volatile controls on magma ascent and eruption, in *The State of the Planet: Frontiers and Challenges in Geophysics*, edited by R. S. J. Sparks, and C. J. Hawkesworth, pp. 109–124, AGU, Washington, D. C., doi:10.1029/150GM10.

Chabot, N. L., B. W. Denevi, S. L. Murchie, C. D. Hash, C. M. Ernst, D. T. Blewett, H. Nair, N. R. Laslo, and S. C. Solomon (2016), Mapping Mercury: Global imaging strategy and products from the MESSENGER mission, *Lunar Planet. Sci.*, *47*, abstract 1256.

Crater Analysis Techniques Working Group (1979), Standard techniques for presentation and analysis of crater size-frequency data, *Icarus*, *37*, 467–474, doi:10.1016/0019-1035(79)90009-5.

Denevi, B. W., et al. (2009), The evolution of Mercury's crust: A global perspective from MESSENGER, *Science*, *324*, 613–618, doi:10.1126/science.1172226.

Denevi, B. W., et al. (2013), The distribution and origin of smooth plains on Mercury, *J. Geophys. Res. Planets*, *118*, 891–907, doi:10.1002/jgre.20075.

Elkins-Tanton, L. T., and B. H. Hager (2005), Giant meteoroid impacts can cause volcanism, *Earth Planet. Sci. Lett.*, *239*, 219–232, doi:10.1016/j.epsl.2005.07.029.

Evans, A. J., S. M. Brown, and S. C. Solomon (2015), Characteristics of early mantle convection and melting on Mercury, *Lunar Planet. Sci.*, *46*, abstract 2414.

Fassett, C. I., J. W. Head, D. T. Blewett, C. R. Chapman, J. L. Dickson, S. L. Murchie, S. C. Solomon, and T. R. Watters (2009), Caloris impact basin: Exterior geomorphology, stratigraphy, morphometry, radial sculpture, and smooth plains deposits, *Earth Planet. Sci. Lett.*, *285*, 297–308, doi:10.1016/j.epsl.2009.05.022.

Fassett, C. I., S. J. Kadish, J. W. Head, S. C. Solomon, and R. G. Strom (2011), The global population of large craters on Mercury and comparison with the Moon, *Geophys. Res. Lett.*, *38*, L10202, doi:10.1029/2011GL047294.

Fassett, C. I., et al. (2012), Large impact basins on Mercury: Global distribution, characteristics, and modification history from MESSENGER orbital data, *J. Geophys. Res.*, *117*, E00L08, doi:10.1029/2012JE004154.

Ferrari, S., M. Massironi, S. Marchi, P. K. Byrne, C. Klimczak, E. Martellato, and G. Cremonese (2014), Age relationships of the Rembrandt basin and Enterprise Rupes, Mercury, in *Volcanism and Tectonism Across the Inner Solar System*, vol. 401, edited by T. Platz, et al., pp. 159–172, Geol. Soc. London Spec. Publ., doi:10.1144/SP401.20.

Glazner, A. F. (1991), Plutonism, oblique subduction, and continental growth: An example from the Mesozoic of California, *Geology*, *19*, 784–786, doi:10.1130/0091-7613(1991)019<0784:POSACG>2.3.CO;2.

Glickson, A. Y. (2004), Impacts do not initiate volcanic eruptions: Eruptions close to the crater: Comment and reply, *Geology*, *32*, e48, doi:10.1130/0091-7613-32.1.e48.

Goudge, T. A., et al. (2014), Global inventory and characterization of pyroclastic deposits on Mercury: New insights into pyroclastic activity from MESSENGER orbital data, *J. Geophys. Res. Planets*, *119*, 635–658, doi:10.1002/2013JE004480.

Hamilton, W. B. (1995), Subduction systems and magmatism, in *Volcanism Associated with Extension to Consuming Plate Margins*, vol. 81, edited by J. R. Smellie, pp. 3–28, Geol. Soc. London Spec. Publ., London.

Hawkins, S. E., III, et al. (2007), The Mercury Dual Imaging System on the MESSENGER spacecraft, *Space Sci. Rev.*, *131*, 247–338, doi:10.1007/s11214-007-9266-3.

Head, J. W., et al. (2008), Volcanism on Mercury: Evidence from the first MESSENGER flyby, *Science*, *321*, 69–72, doi:10.1126/science.1159256.

Head, J. W., et al. (2009a), Volcanism on Mercury: Evidence from the first MESSENGER flyby for extrusive and explosive activity and the volcanic origin of plains, *Earth Planet. Sci. Lett.*, *285*, 227–242, doi:10.1016/j.epsl.2009.03.007.

Head, J. W., et al. (2009b), Evidence for intrusive activity on Mercury from the first MESSENGER flyby, *Earth Planet. Sci. Lett.*, *285*, 251–262, doi:10.1016/j.epsl.2009.03.008.

Head, J. W., et al. (2011), Flood volcanism in the northern high latitudes of Mercury revealed by MESSENGER, *Science*, *333*, 1853–1856, doi:10.1126/science.1211997.

Hiesinger, H., J. W. Head, U. Wolf, R. Jaumann, and G. Neukum (2003), Ages and stratigraphy of mare basalts in Oceanus Procellarum, Mare Nubium, Mare Cognitum, and Mare Insularum, *J. Geophys. Res.*, *108*(E7), 5065, doi:10.1029/2002JE001985.

Holsapple, K. A., and K. R. Housen (2007), A crater and its ejecta: An interpretation of deep impact, *Icarus*, *187*, 345–356, doi:10.1016/j.icarus.2006.08.035.

Ivanov, B. A., and H. J. Melosh (2003), Impacts do not initiate volcanic eruptions: Eruptions close to the crater, *Geology*, *31*, 869–872, doi:10.1130/G19669.1.

Ivanov, M. A., and J. W. Head (2013), The history of volcanism on Venus, *Planet. Space Sci.*, *84*, 66–92, doi:10.1016/j.pss.2013.04.018.

Kerber, L. A., J. W. Head, S. C. Solomon, S. L. Murchie, D. T. Blewett, and L. Wilson (2009), Explosive volcanic eruptions on Mercury: Eruption conditions, magma volatile content, and implications for interior volatile abundances, *Earth Planet. Sci. Lett.*, *285*, 263–271, doi:10.1016/j.epsl.2009.04.037.

Kerber, L. A., J. W. Head, D. T. Blewett, S. C. Solomon, L. Wilson, S. L. Murchie, M. S. Robinson, B. W. Denevi, and D. L. Domingue (2011), The global distribution of pyroclastic deposits on Mercury: The view from MESSENGER flybys 1–3, *Planet. Space Sci.*, *59*, 1895–1909, doi:10.1016/j.pss.2011.03.020.

Klimczak, C. (2015), Limits on the brittle strength of lithospheres undergoing global contraction, *J. Geophys. Res. Planets*, *120*, 2135–2151, doi:10.1002/2015JE004851.
Klimczak, C., P. K. Byrne, S. C. Solomon, F. Nimmo, T. R. Watters, B. W. Denevi, C. M. Ernst, and M. E. Banks (2013), The role of thrust faults as conduits for volatiles on Mercury, *Lunar Planet. Sci.*, *44*, abstract 1390.
Kneissl, T., S. van Gasselt, and G. Neukum (2011), Map-projection-independent crater size–frequency determination in GIS environments—New software tool for ArcGIS, *Planet. Space Sci.*, *59*, 1243–1254, doi:10.1016/j.pss.2010.03.015.
Le Feuvre, M., and M. A. Wieczorek (2011), Nonuniform cratering of the Moon and a revised crater chronology of the inner solar system, *Icarus*, *214*, 1–20, doi:10.1016/j.icarus.2011.03.010.
Marchi, S., S. Mottola, G. Cremonese, M. Massironi, and E. Martellato (2009), A new chronology for the Moon and Mercury, *Astron. J.*, *137*, 4936–4948, doi:10.1088/0004-6256/137/6/4936.
Marchi, S., M. Massironi, G. Cremonese, E. Martellato, L. Giacomini, and L. M. Prockter (2011), The effects of the target material properties and layering on the crater chronology: The case of Raditladi and Rachmaninoff basins on Mercury, *Planet. Space Sci.*, *59*, 1968–1980, doi:10.1016/j.pss.2011.06.007.
Marchi, S., C. R. Chapman, C. I. Fassett, J. W. Head, W. F. Bottke, and R. G. Strom (2013), Global resurfacing of Mercury 4.0–4.1 billion years ago by heavy bombardment and volcanism, *Nature*, *499*, 59–61, doi:10.1038/nature12280.
Marrett, R., and S. H. Emerman (1992), The relations between faulting and mafic magmatism in the Altiplano-Puna plateau (central Andes), *Earth Planet. Sci. Lett.*, *112*, 53–59, doi:10.1016/0012-821X(92)90006-H.
Massironi, M., G. Cremonese, S. Marchi, E. Martellato, S. Mottola, and R. J. Wagner (2009), Mercury's geochronology revised by applying model production function to Mariner 10 data: Geological implications, *Geophys. Res. Lett.*, *36*, L21204, doi:10.1029/2009GL040353.
Michael, G. G., and G. Neukum (2010), Planetary surface dating from crater size–frequency distribution measurements: Partial resurfacing events and statistical age uncertainty, *Earth Planet. Sci. Lett.*, *294*, 223–229, doi:10.1016/j.epsl.2009.12.041.
Michael, G. G., T. Kneissl, and A. Neesemann (2016), Planetary surface dating from crater size-frequency distribution measurements: Poisson timing analysis, *Icarus*, *277*, 279–285, doi:10.1016/j.icarus.2016.05.019.
Michel, N. C., S. A. Hauck II, S. C. Solomon, R. J. Phillips, J. H. Roberts, and M. T. Zuber (2013), Thermal evolution of Mercury as constrained by MESSENGER observations, *J. Geophys. Res. Planets*, *118*, 1033–1044, doi:10.1002/jgre.20049.
Murchie, S. L., et al. (2008), Geology of the Caloris basin, Mercury: A view from MESSENGER, *Science*, *321*, 73–76, doi:10.1126/science.1159261.
Neukum, G., B. A. Ivanov, and W. K. Hartmann (2001), Cratering records in the inner solar system in relation to the lunar reference system, *Space Sci. Rev.*, *96*, 55–86, doi:10.1023/A:1011989004263.
Ostrach, L. R., M. S. Robinson, J. L. Whitten, C. I. Fassett, R. G. Strom, J. W. Head, and S. C. Solomon (2015), Extent, age, and resurfacing history of the northern smooth plains on Mercury from MESSENGER observations, *Icarus*, *250*, 602–622, doi:10.1016/j.icarus.2014.11.010.
Prockter, L. M., et al. (2010), Evidence for young volcanism on Mercury from the third MESSENGER flyby, *Science*, *329*, 668–671, doi:10.1126/science.1188186.
Roberts, J. H., and O. S. Barnouin (2012), The effect of the Caloris impact on the mantle dynamics and volcanism of Mercury, *J. Geophys. Res.*, *117*, E02007, doi:10.1029/2011JE003876.
Robinson, M. S., et al. (2008), Reflectance and color variations on Mercury: Regolith processes and compositional heterogeneity, *Science*, *321*, 66–69, doi:10.1126/science.1160080.
Solomon, S. C. (1978), On volcanism and thermal stresses on one-plate planets, *Geophys. Res. Lett.*, *5*, 461–464, doi:10.1029/GL005i006p00461.
Spudis, P. D., and J. E. Guest (1988), Stratigraphy and geologic history of Mercury, in *Mercury*, edited by F. Vilas, C. R. Chapman, and M. S. Matthews, pp. 118–164, Univ. of Ariz. Press, Tucson, Ariz.
Strom, R. G., and G. Neukum (1988), The cratering record on Mercury and the origin of impacting objects, in *Mercury*, edited by F. Vilas, C. R. Chapman, and M. S. Matthews, pp. 336–373, Univ. of Ariz. Press, Tucson, Ariz.
Strom, R. G., N. J. Trask, and J. E. Guest (1975), Tectonism and volcanism on Mercury, *J. Geophys. Res.*, *80*, 2478–2507, doi:10.1029/JB080i017p02478.
Strom, R. G., C. R. Chapman, W. J. Merline, S. C. Solomon, and J. W. Head (2008), Mercury cratering record viewed from MESSENGER's first flyby, *Science*, *321*, 79–81, doi:10.1126/science.1159317.
Strom, R. G., M. E. Banks, C. R. Chapman, C. I. Fassett, J. A. Forde, J. W. Head, M. J. Merline, L. M. Prockter, and S. C. Solomon (2011), Mercury crater statistics from MESSENGER flybys: Implications for stratigraphy and resurfacing history, *Planet. Space Sci.*, *59*, 1960–1967, doi:10.1016/j.pss.2011.03.018.
Thomas, R. J., D. A. Rothery, S. J. Conway, and M. Anand (2014), Long-lived explosive volcanism on Mercury, *Geophys. Res. Lett.*, *41*, 6084–6092, doi:10.1002/2014GL061224.
Tosi, N., M. Grott, A.-C. Plesa, and D. Breuer (2013), Thermochemical evolution of Mercury's interior, *J. Geophys. Res. Planets*, *118*, 2474–2487, doi:10.1002/jgre.20168.
Trask, N. J., and J. E. Guest (1975), Preliminary geologic terrain map of Mercury, *J. Geophys. Res.*, *80*, 2461–2477, doi:10.1029/JB080i017p02461.
Watanabe, T., T. Koyaguchi, and T. Seno (1999), Tectonic stress controls on ascent and emplacement of magmas, *J. Volcanol. Geotherm. Res.*, *91*, 65–78, doi:10.1016/S0377-0273(99)00054-2.
Whitten, J. L., J. W. Head, B. W. Denevi, and S. C. Solomon (2014), Intercrater plains on Mercury: Insights into unit definition, characterization, and origin from MESSENGER datasets, *Icarus*, *241*, 97–113, doi:10.1016/j.icarus.2014.06.013.
Wilson, L., and J. W. Head (2008), Volcanism on Mercury: A new model for the history of magma ascent and eruption, *Geophys. Res. Lett.*, *35*, L23205, doi:10.1029/2008GL035620.